PHASE CHANGES IN NI-TI UNDER LASER SHOCK LOADING

R.E. Hackenberg[1], D.C. Swift[2], J.C. Cooley[1], K.C. Chen[3], D.J. Thoma[1], D.L. Paisley[2] and A. Hauer[4]

[1]Materials Science and Technology Division (MST-6), MS G770, Los Alamos National Laboratory, Los Alamos, NM 87545, USA

[2]Physics Division (P-24), MS E526, Los Alamos National Laboratory, Los Alamos, NM 87545, USA

[3] Materials Engineering Department, California Polytechnic State University, San Luis Obispo, CA 93407, USA

[4]Physics Division (P-DO), MS E527, Los Alamos National Laboratory, Los Alamos, NM 87545, USA

Near-equiatomic Ni-Ti, known for its shape memory behavior, can decompose to martensitic phases and/or second phase compounds. This phase competition is investigated in Ni_xTi_{100-x} ($49<x<55$) in as-quenched (AQ) and shock-loaded states. Dynamic loading was done with direct drive laser pulses of nanosecond duration; shocked samples were recovered for analysis. Unexpectedly, the lowest-Ni alloy (x = 48.9) showed reversion of B19' martensite (present in the AQ state) to the B2 parent phase upon loading, attributed to shock-induced heating. Higher-Ni alloys (x = 50.7, 52.6, 54.5, 54.6) showed Ni_4Ti_3 but no martensite in the AQ state, consistent with resistivity and dilatometry results which showed no hysteresis indicative of first order phase changes over $1.9\ K<T<1273\ K$. Shock loading these alloys formed no martensite, but the Ni_4Ti_3 amounts (present in the AQ state) did change upon loading, indicating the importance of shock-induced heating. A thermodynamically complete equation of state (EOS) for NiTi in its B2 (CsCl) structure was generated by ab initio quantum mechanical calculations. This was tested by performing laser-launched flyer experiments, which showed consistency with the theoretical EOS, validating its use in the prediction of dynamic loading histories in the samples during direct drive loading.

INTRODUCTION

Martensitic transformations are responsible for the shape memory effect exhibited by various alloys (1), such as those based on near-equiatomic Ni-Ti (2), the most widely used shape memory alloy. The B2 parent phase in Ni-Ti can decompose not only in a diffusionless fashion to rhombohedral (R-Phase) and monoclinic (B19') martensitic phases, but also diffusionally to intermetallic compounds (Ni_3Ti, Ni_3Ti_2 and Ni_4Ti_3) (3) when the composition deviates from ideal B2 stoichiometry ($Ni_{50}Ti_{50}$). The interaction between these decomposition paths greatly affects the shape memory behavior in ways that are not yet fully understood. This work studies several Ni-Ti alloys to examine the phase evolution as a function of composition and dynamic loading path (done by direct-drive laser shock-loading).

The mechanism of martensitic transformations, so critical for the shape memory effect, is also incompletely understood (4,5), due in part to the high growth rate of martensitic product units (6). The laser-based technique used here may provide answers to questions regarding the mechanism of martensitic transformations, as ultra-short pulse durations restrict the time available for the stress-assisted growth of martensite units (7) in the temperature range $M_s < T < M_s^{\sigma}$, where M_s^{σ} is the highest temperature where martensite can be stress-induced. Nanosecond stress pulses, inaccessible from traditional gas-gun techniques used in Fe-base (8,9,10) and Ni-Ti (11) alloys, allow the nucleation site and incubation time of the first-formed martensite units to be probed.

To predict the loading history of the samples shocked by direct-drive laser, quantum mechanical calculations of the equation of state for Ni-Ti in the B2 phase (CsCl structure) were carried out and compared with the results of laser-driven flyer plate experiments on Ni-Ti alloys.

ALLOY PREPARATION AND THE AS-QUENCHED STATE

Several binary Ni-Ti alloys were arc melted from high-purity Ni and Ti under argon; the ingots were homogenized 50 hours at 1100°C under argon, and water-quenched. Alloys with 48.9, 50.7, 52.6, 54.5 and 54.6 at. % Ni were made for laser direct-drive shock experiments, for which 6 mm Ø discs were prepared by electro-discharge machining, grinding and polishing. (These compositions were determined by chemical analysis.) For the laser-launched flyer experiments, alloys with 52.0 and 54.2 at.% Ni were made, from which full and half discs of 5 mm Ø were prepared for flyer and target specimens, respectively. As-quenched (AQ) samples were characterized by optical microscopy, TEM, x-ray diffraction (CuKα radiation), dilatometry, DSC and resistivity. The thermal path taken during resistivity scans was: 298K to 400K to 1.9K to 400K and finally back to 298K.

X-ray diffraction (XRD) of the as-quenched (AQ) samples (Fig. 1) shows monoclinic B19' martensite and perhaps some B2 in 48.9 Ni. (Note that the actual B2 and B19' peaks in the XRD plots may not coincide exactly with their line labels due to off-stoichiometric alloy compositions, as the labels correspond to $Ni_{50}Ti_{50}$.) All other alloys exhibited mixtures of B2 and Ni_4Ti_3 (which presumably formed during quenching); no peaks for either R-Phase or B19' martensite were seen. Although Ni_4Ti_3 is metastable, it has the most rapid precipitation kinetics of the Ni-rich intermetallics (3); hence, its presence in the AQ state is not surprising. Its presence was confirmed by selected area diffraction in the TEM.

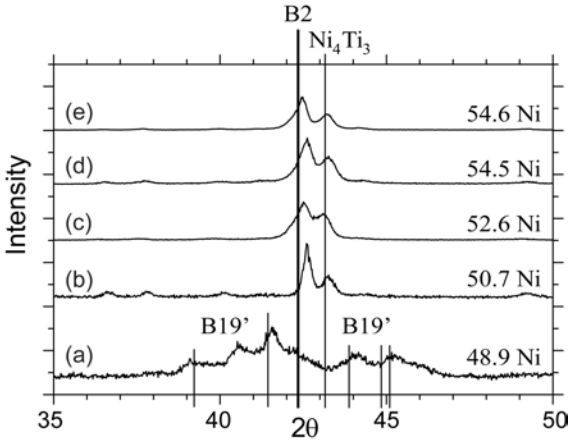

FIGURE 1. X-Ray Diffraction of the As-Quenched Ni-Ti Alloys. Vertical lines indicate the peaks corresponding to various phases.

Resistivity (Figs. 2-3), dilatometry and DSC all showed hysteresis near room temperature in 48.9 Ni. This indicates a first order phase transformation, known to be martensitic from XRD and the literature. As expected for near-equiatomic Ni-Ti, the hysteresis is small (tens of degrees). The martensite start temperature (M_s) is above ambient, explaining why B19' martensite is present in the AQ state (Fig. 1). The martensite finish (M_f) is sub-ambient, consistent with the traces of B2 in Fig. 1. These techniques all show no hysteresis between 1.9 K and 1273 K in 50.7, 52.6, 54.5 and 54.6 Ni. Given that martensite is found at lower temperatures in off-stoichiometric Ni-rich alloys, a sub-ambient martensitic transition is possible for the higher Ni alloys, but resistivity (e.g., Fig. 4) shows no evidence of this. The negative temperature dependence of resistivity in the 50.7 Ni alloy (Fig. 4) was found in similar studies (12) and was attributed

to formation of nanometer-scale scattering centers, namely fine-scale Ni_4Ti_3 precipitates. This negative temperature dependence was not found in all these alloys, though.

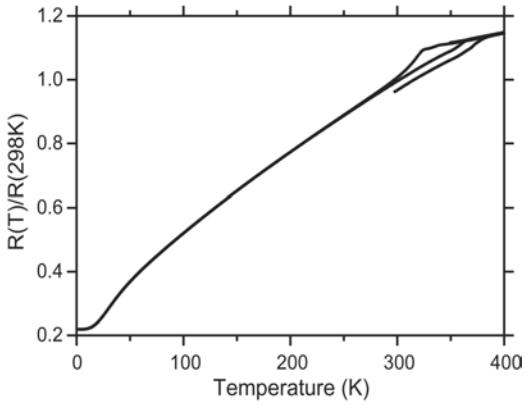

FIGURE 2. Resistivity of 48.9 Ni. R(298K)=1.92 x 10^{-4} ohm-cm.

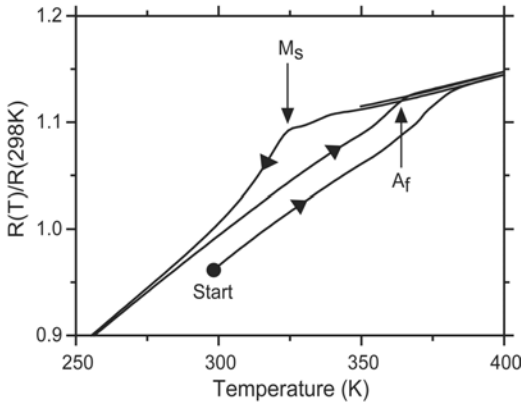

FIGURE 3. Fig. 2 expanded to show the martensitic hysteresis. M_s is 323K, A_f is 363K and M_f is below 298K, near the intersection of the cooling and heating curves. Arrows indicate the thermal path.

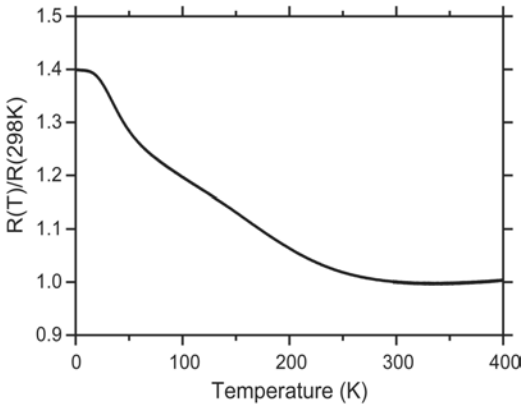

FIGURE 4. Resistivity of 50.7 Ni, showing no hysteresis and also a negative temperature dependence. R(298K)=1.07 x 10^{-4} ohm-cm.

SHOCK AND RECOVERY EXPERIMENTS

Samples were subjected to dynamic loading by direct-drive laser, then recovered to analyze the effect of shock loading and composition on the microstructure and phases present. The samples used in these experiments were ~100 microns thick. Ten experiments were performed: two each on five different alloy compositions.

The TRIDENT laser was used to induce pressure pulses by illuminating the front surface of the sample directly. The pulse length in these experiments was 1.8 or 3.6 ns, and the pulse energies varied from 20 to 60 J. The opposite (back) surface of the sample was monitored with laser Doppler velocimetry, using a line-imaging VISAR system. In most experiments, the sample was mounted on a sapphire window, intended to decelerate the shocked sample in an essentially 1D fashion, making it easier to correlate the loading history with the microstructure. In three experiments no window was used. The sample (and window, if used) was mounted in a clamp which held it around its entire edge. These experiments were carried out in an evacuated target chamber. (Fig. 5).

The ab initio EOS was used in hydrocode simulations to estimate the loading history at each point in the sample. According to the simulations, the laser pulse produced a slowly-decaying triangular wave. Peak pressures were 7-21 GPa.

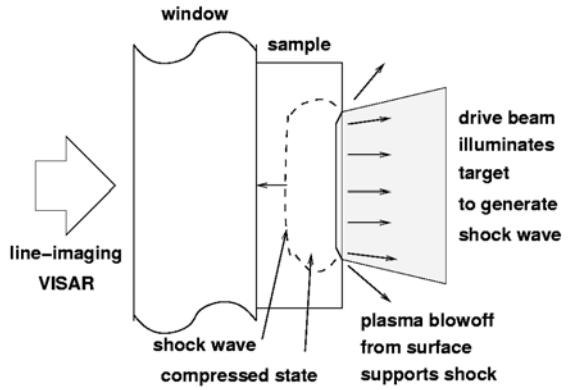

FIGURE 5. Schematic of TRIDENT direct drive experiments.

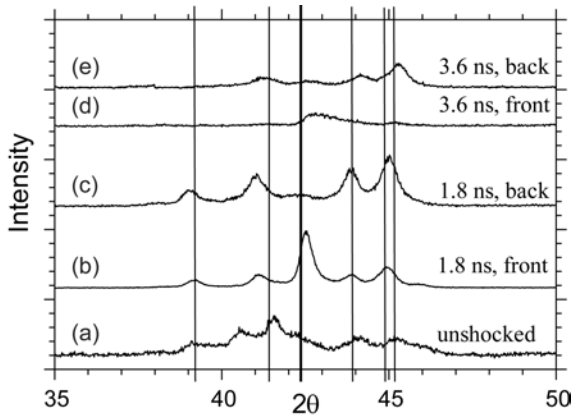

FIGURE 6. XRD of AQ (a) and shocked (b-e) 48.9 Ni. The thick vertical line corresponds to the parent B2 phase; the thinner lines to the B19' martensite, which has disappeared from the front faces of the samples after loading. The front faces of the discs (b,d) were the ones impacted by the laser pulse; VISAR measurements were taken from the corresponding back faces from the same shots (c,e). The 1st (b,c) and 2nd (d,e) shots had initial shock pressures of 8 and 7 GPa, respectively. The 2nd shot (d,e) used no window.

X-ray diffraction (XRD) characterized the phase distributions (i.e., B2, martensite and compounds) in the shocked specimens. In 48.9 Ni (Fig. 6), the front faces of the shocked discs showed reversion of the B19' martensite to B2, while the back faces showed little change. This reverse transformation was unexpected, as uniaxial compression and tension in the shocked region are expected to promote stress-assisted martensite formation below M_s^σ (and substructural rearrangement of any existing martensite), not its dissolution (7). The likeliest explanation for this reversion is the thermal effects within the shocked region: the temperature rise (calculated from the EOS) takes the sample to 300-350°C, in the single phase B2 region well above M_s^σ and A_f, causing B19' reversion. Martensite fails to reappear upon cooling to ambient by a reduction in M_s (and M_s^σ) due to shock-induced generation of defects, which stabilize the B2 against shearing to B19'. Why such defects would not stimulate strain-induced martensite (13) (between $M_s^\sigma<T<M_d$) is not clear. The behavior at the back face depends on how much the shock wave decays by the time it reaches the back face; preliminary calculations indicate that for these pulses, the peak stress amplitude decays by more than 50%; this might explain the lack of change (with respect to the baseline AQ state) in terms of reduced defect generation which would cause a lesser reduction in M_s (and M_s^σ), allowing the B19' phase to re-form upon cooling.

The other alloys (50.7, 52.6, 54.5 and 54.6 Ni), initially free of martensite, showed no martensite formation during shock loading. This is consistent with the lack of hysteresis in the resistivity: the fact that a martensitic transformation cannot be induced by lowering the temperature down to 2 K indicates that the (moderate) stress states produced during these shock loading experiments are unlikely to do so either. However, shock loading caused changes in the amounts of the Ni_4Ti_3 intermetallic phase. Such changes can only come about as a result of diffusion of Ni and Ti; it is unlikely that Ni_4Ti_3 can precipitate or dissolve in a compositionally-invariant fashion and still be thermodynamically feasible. This gives the strongest evidence that thermal effects within the shock wave outweigh the stress effects in the alloys and shock conditions examined, consistent with the tentative interpretation of the 48.9 Ni alloy behavior.

50.7 Ni (Fig. 7) showed dissolution of Ni_4Ti_3 into the B2 solid solution in both shots and on both sides of the discs in each shot. The 52.6, 54.5 and 54.6 Ni (Fig. 8) alloys all showed either increased Ni_4Ti_3 or little change. It also showed what could be a new phase, suggested by a new peak immediately to the right of the Ni_4Ti_3 peak in some cases. This peak could not be indexed to any known martensite

or intermetallic phase expected for these alloys. No systematic correlations of the phase change behavior could be made with the front and back faces.

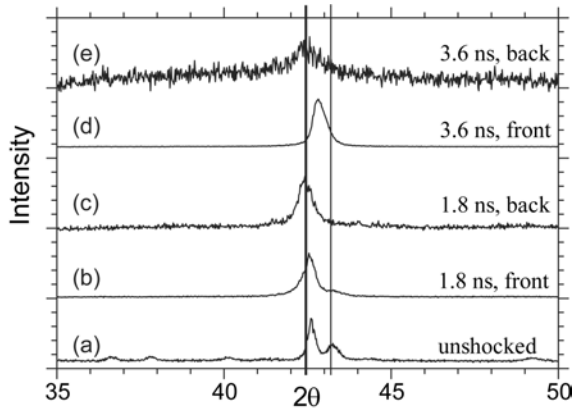

FIGURE 7. XRD of AQ (a) and shocked (b-e) 50.7 Ni. The thick vertical line denotes B2; the thin line denotes Ni_4Ti_3, which is gone after loading. The shots had initial shock pressures of 15 GPa (b,c) and 7 GPa (d,e). The 2nd shot (d,e) used no window.

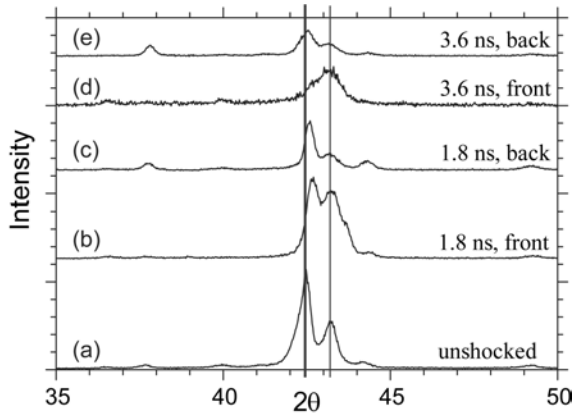

FIGURE 8. XRD scans of AQ (a) and shocked (b-e) 54.6 Ni. The thick vertical line denotes B2; the thin line denotes Ni_4Ti_3, which increased on the front faces after loading. The shots had initial shock pressures of 19 GPa (b,c) and 21 GPa (d,e), respectively.

In all alloys (except for 49.8 Ni), the temperature rise during loading (however brief) could influence the Ni_4Ti_3 distribution in one of two ways. In a weakly off-stoichiometric alloy such as 50.7 Ni, the temperature rise would exceed the metastable solvus boundary for Ni_4Ti_3, causing its dissolution; cooling to ambient after shock decay would be rapid enough to avoid Ni_4Ti_3 re-precipitation. The 52.6, 54.5 and 54.6 Ni, on the other hand, would have a much higher metastable solvus temperature for Ni_4Ti_3 as well as a much greater thermodynamic driving force for its precipitation. Therefore, the shock-induced heating would act like an aging heat treatment, allowing more Ni and Ti diffusion, which grows existing Ni_4Ti_3 precipitates and nucleates new ones, all of which are retained on the post-shock quench.

Pursuant to the goal of better understanding martensitic transformation mechanisms, the results of this initial survey suggest several changes in the experiments for future work. As only one of the five alloys used in direct-drive experiments showed any sign of martensite, more precise tailoring of alloy compositions is needed, given the strong influence of composition on the critical temperatures for martensite. The initial shock pressures (which determine the temperature rise within the shocked region) will also have to be lowered to promote the stress-assisted formation and retention of martensite, which require that stress effects within the shocked region dominate over thermal effects.

EQUATION OF STATE DETERMINATION

A thermodynamically complete equation of state (EOS) is needed in order to understand the dynamic loading applied to a sample, and hence interpret the microstructure of recovered specimens. No relevant EOS for Ni-Ti alloys have been published, so the EOS was determined by theory and experiment.

An ab initio EOS was calculated using quantum mechanics, by a variant of a method applied previously to several elements (14). The frozen-ion cold curve was estimated for Ni-Ti in the B2 (CsCl) structure by finding the ground state energy of the outer electrons with respect to ab initio pseudopotentials for Ni and Ti. The variation of Grueneisen's Gamma with compression was estimated from the cold curve by fitting functional forms and applying the Dugdale-Macdonald formula. Assuming a constant value for the specific heat capacity, a thermodynamically complete EOS was generated. Because of the intrinsic limitations of the local density approximation used to represent the exchange-correlation energy of the outer electrons, the ab initio EOS overpredicted the lattice

spacing at STP by ~1%. This discrepancy was corrected by adding a constant pressure offset to the EOS.

The theoretical EOS was tested, and a basic constitutive model obtained, by performing laser-launched flyer experiments with laser Doppler velocimetry (VISAR) diagnostics. Flyers made from copper or Ni-Ti were mounted on a substrate consisting of PMMA coated with thin (~micron) layers of materials to absorb the laser energy, confine the plasma, and insulate the flyer from heating. The flyers were between 50 and 200 microns thick.

The TRIDENT laser at Los Alamos was used to launch the flyers. Pulses ~600 ns long in the infra-red were used, allowing the flyers to be launched without shocking up, spalling or significant ringing. Flyer speeds up to ~600 m/s were obtained.

The flyers were impacted against Ni-Ti targets, attached to PMMA windows. The target typically covered half of the area of the flyer, giving space for the flyer speed to be measured with the VISAR. The back surface of the target - releasing into the window or into vacuum - was also monitored with the VISAR. Wave profiles at the surface of the target provided EOS and strength information. In the case of Ni-Ti flyers, the deceleration on impact with the window provided a point on the principal Hugoniot.

The EOS data obtained were reasonably consistent with the theoretical EOS, though the measured shock states exhibited more structure, suggesting that a phase transition may have occurred (Fig. 9). The degree of agreement validated the use of the simple theoretical EOS in the prediction of dynamic loading histories at different positions in the samples.

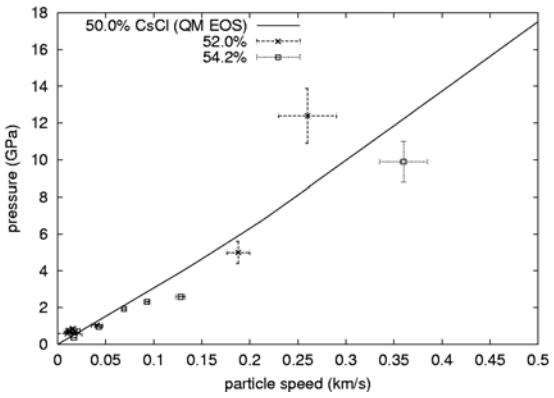

FIGURE 9. Comparison between theoretical EOS and data from flyer impact experiments on two compositions of Ni-Ti alloy.

CONCLUSIONS

The direct-drive laser shock technique allowed Ni-Ti samples to be loaded with nanosecond-scale pulses and recovered without undue disruption to the microstructure. Post-shock characterization revealed microstructural changes attributed to the dominance of thermal effects over stress effects within the shocked region, as evidenced by the reversion of B19' martensite to the B2 parent phase in 48.9 Ni and the changes in the amount of Ni_4Ti_3 in the other (Ni-rich) alloys. Thus, the competition between the parent, martensitic and intermetallic phases in the as-quenched and shock-loaded states was strongly dependent on alloy composition and loading history.

The ab initio quantum mechanical method produced a complete EOS for Ni-Ti alloy in the B2 (CsCl) structure. The EOS was tested against laser-launched flyer experiments, which were appropriate in terms of pressure range and time-scales for the direct-drive experiments.

ACKNOWLEDGMENTS

This work was supported by a LDRD grant funded under the auspices of the U.S. Department of Energy under contract W-7405-ENG-36. We would like to acknowledge the contributions of the TRIDENT team, Andrew Forsman for his help in operating the line VISAR, and P. Ambalal-Patel, L.B. Dauelsburg, W.L. Hults A.M. Kelly and P.A.

Papin for assistance with alloy and specimen preparation.

REFERENCES

1. Wei, Z.G., Sandstrom, R. and Miyazaki, S., J. Mater. Sci. **33**, 3743 (1998).
2. Saburi, T., *Ti-Ni Shape Memory Alloys*, "Shape Memory Materials", Otsuka, K. and Wayman, C.M. -eds., Cambridge, 49 (1998).
3. Nishida, M., Wayman, C.M. and Honma, T., Metall. Trans. A **17A**, 1505 (1986).
4. Kaufman, L. and Cohen, M., Progress in Metal Physics **7**, 165 (1958).
5. Olson, G.B. and Owen, W.S. -eds., "Martensite", ASM, Metals Park, OH (1991).
6. Bunshah, R.F. and Mehl, R.F., Trans. AIME **197**, 1251 (1953).
7. Patel, J.R. and Cohen, M., Acta Metall. **1**, 531 (1953).
8. Thadhani, N.N. and Meyers, M.A., Acta Metall. **34**, 1625 (1986).
9. Chang, S.N. and Meyers, M.A., Acta Metall. **36**, 1085 (1988).
10. Sano, Y., Chang, S.N., Meyers, M.A. and Nemat-Nasser, S., Acta Metall. **40**, 413 (1992).
11. Thakur, A.M., Thadhani, N.N. and Schwarz, R.B., Metall. Trans. A **28A**, 1445 (1997).
12. Somsen, Ch., Zahres, H., Kastner, J., Wasserman, E.F., Kakashita, T. and Saburi, T., Mater. Sci. Eng. A273-275, **310** (1999).
13. Olson, G.B. and Cohen, M., J. Less-Common Metals **28**, 107 (1972).
14. Swift, D.C., G.J. Ackland, A. Hauer and G.A. Kyrala, Phys. Rev. B **64**, 214107 (2001).